Dominant role of soil moisture in mediating carbon and water fluxes in dryland ecosystems

Steven A. Kannenberg ⓘ [1,2] ✉, William R. L. Anderegg ⓘ [3,4], Mallory L. Barnes[5], Matthew P. Dannenberg ⓘ [6] & Alan K. Knapp ⓘ [2]

Drylands exert a strong influence over global interannual variability in carbon and water cycling due to their substantial heterogeneity over space and time. This variability in ecosystem fluxes presents challenges for understanding their primary drivers. Here we quantify the sensitivity of dryland gross primary productivity and evapotranspiration to various hydrometeorological drivers by synthesizing eddy covariance data, remote sensing products and land surface model output across the western United States. We find that gross primary productivity and evapotranspiration derived from eddy covariance are most sensitive to soil moisture fluctuations, with lesser sensitivity to vapour pressure deficit and little to no sensitivity to air temperature or light. We find that remote sensing data accurately capture the sensitivity of eddy covariance fluxes to soil moisture but largely over-predict sensitivity to atmospheric drivers. In contrast, land surface models underestimate sensitivity of gross primary productivity to soil moisture fluctuations by approximately 45%. Amid debates about the role of increasing vapour pressure deficit in a changing climate, we conclude that soil moisture is the primary driver of US dryland carbon–water fluxes. It is thus imperative to both improve model representation of soil water limitation and more realistically represent how atmospheric drivers affect dryland vegetation in remotely sensed flux products.

Dryland ecosystems exert a substantial influence on the global climate system, in part by mediating interannual variability in the strength of the land carbon sink[1,2]. However, drylands are warming faster than the global mean[3] and are expected to continue aridifying in the coming decades[4,5], which could trigger feedbacks that alter or dampen their crucial role in mediating global carbon–water cycling.

These ongoing and future changes to drylands necessitate a robust assessment of the drivers of their carbon and water cycles. However, studying drylands at the necessary spatial and temporal scales to accurately characterize carbon–water fluxes is notoriously challenging. Field research campaigns, for example, typically do not operate at spatial scales large enough to account for the topographical and hydrological variability present in most drylands and seldom last for more than a few consecutive years. Land surface models, while generating spatially continuous estimates of carbon–water fluxes, generally operate at coarse spatial scales and underestimate both the magnitude and variability of dryland fluxes[6,7]. Many remote sensing products also perform poorly in drylands due to the limited ability

[1]Department of Biology, West Virginia University, Morgantown, WV, USA. [2]Department of Biology and Graduate Degree Program in Ecology, Colorado State University, Fort Collins, CO, USA. [3]School of Biological Sciences, University of Utah, Salt Lake City, UT, USA. [4]Wilkes Center for Climate Science and Policy, University of Utah, Salt Lake City, UT, USA. [5]O'Neill School of Public and Environmental Affairs, Indiana University, Bloomington, IN, USA. [6]Department of Geographical and Sustainability Sciences, University of Iowa, Iowa City, IA, USA. ✉e-mail: steven.kannenberg@mail.wvu.edu

of existing satellites to capture dryland heterogeneity, noise introduced from inactive vegetation or soils and weak linkages between vegetation activity and reflectance[8]. As such, important ecological questions remain unresolved: (1) Are dryland fluxes more sensitive to fluctuations in atmospheric drivers (for example, temperature, light, evaporative demand) or soil moisture? And (2) how sensitive are dryland fluxes to variation in shallow versus deep soil moisture pools? Answering these questions is increasingly pertinent as air temperature and atmospheric water demand rises[9] and soil moisture decreases[10]. If atmospheric aridity or temperature is the primary driver of dryland fluxes, climate change may accelerate dryland aridification or amplify feedback mechanisms that diminish their capacity to absorb atmospheric CO_2[11].

A multi-scale, multi-method synthesis holds promise towards characterizing dryland fluxes at frequent temporal scales and small spatial scales. In particular, eddy covariance (EC) data are valuable for linking hydrometeorological drivers to ecosystem function[12] given their long-term monitoring capability, high temporal frequency and coverage across numerous dryland biome types. Existing networks of EC observations now contain multi-decadal datasets of ecosystem fluxes and meteorological conditions, enabling an assessment of ecosystem fluxes across a wide range of interannual weather variability. However, the degree to which the drivers of EC fluxes are accurately represented in remotely sensed or modelled data products remains unknown, which limits our ability to understand linkages between hydrometeorological drivers and dryland ecosystem function at regional or global scales.

Here we characterized the drivers of dryland carbon and water cycling, including their relative sensitivities to atmospheric drivers versus soil moisture pools at different depths, by leveraging a network of EC towers across the western United States (Extended Data Fig. 1 and Extended Data Table 1). Efforts to quantify the drivers of ecosystem fluxes at such a high frequency are relatively rare, despite the outsized importance of meteorological 'hot moments' in driving dryland carbon–water cycling broadly[13]. We then evaluated the ability of multiple remotely sensed data products and a suite of land surface models to capture these dynamics. This cross-scale evaluation of dryland ecosystem function can help pinpoint regions most susceptible to current and future changes in climate.

Soil moisture is the dominant driver of carbon–water fluxes

To quantify the drivers of dryland gross primary productivity (GPP) and evapotranspiration (ET), we calculated the sensitivity of daily fluxes to various hydrometeorological drivers using Pearson's and Spearman's correlation coefficients, along with relative weight analysis (RWA)[14]. These analyses revealed that GPP was highly sensitive to fluctuations in soil water availability across the entire soil profile (Fig. 1a). At most sites, GPP significantly increased in concert with soil moisture (mean correlation coefficient ranging from 0.33 and 0.49 across soil layers), whereas it significantly decreased with increasing vapour pressure deficit (VPD, mean coefficient of −0.22). GPP responded much less strongly to air temperature (TA) and light (photosynthetic photon flux density, PPFD), with mean coefficients of −0.08 and −0.01, respectively. Indeed, at the sites where soil moisture was measured, only the wettest site had a higher sensitivity of GPP to any atmospheric driver than to soil moisture (Extended Data Fig. 2). ET was also highly responsive to fluctuations in soil moisture and was weakly associated with variability in atmospheric drivers (Fig. 1a and Extended Data Fig. 3). However, ET was more sensitive to soil moisture in shallow layers than in deep layers, probably due to evaporation from the soil surface being a sizeable component of ET[15]. The high sensitivity of GPP and ET to soil moisture was also evident at half-hourly (Fig. 2a), weekly (Fig. 2b) and monthly (Fig. 2c) timescales. We found similar results when using RWA, which accounts for collinearity in predictor variables (Extended Data Fig. 4 and Methods) and the Spearman's correlation coefficient which better
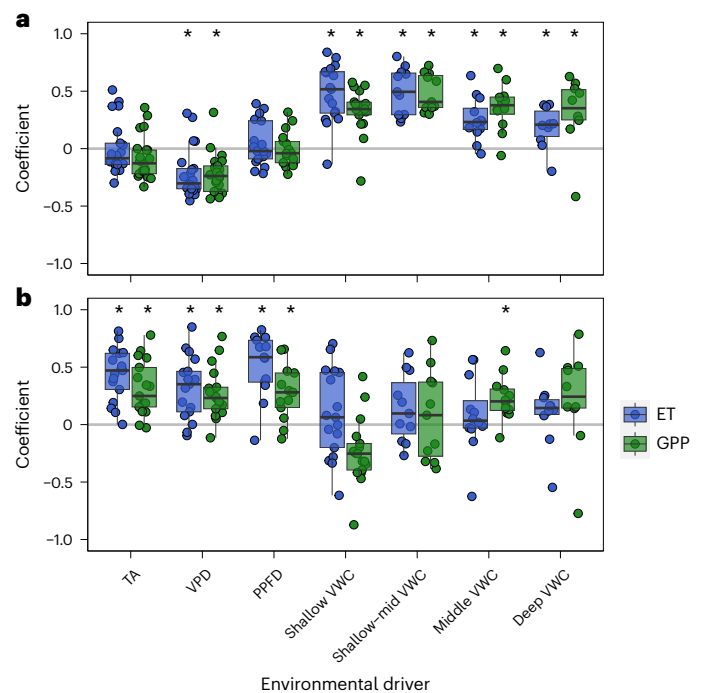

Fig. 1 | Correlation coefficients between daily GPP/ET and environmental drivers. a,b, Correlation coefficients between daily GPP/ET and environmental drivers, calculated using the full dataset (**a**) and only the 10% wettest mean soil moisture observations (**b**). Environmental drivers include TA, VPD, PPFD and various layers of volumetric water content (VWC; Methods provide the depths included in each layer). Asterisks indicate where coefficients are significantly different from zero ($\alpha = 0.05$). Box plot lines represent the interquartile range and median, whereas the whiskers represent 1.5 times the interquartile range.

assesses the strength of nonlinear relationships (Extended Data Fig. 5). Together, these analyses provide robust evidence of the high sensitivity of dryland GPP and ET to soil moisture across temporal scales.

Whereas soil moisture was the largest driver of GPP and ET across these dryland sites, atmospheric drivers may become more important during periods when water supply is abundant. This is because the alleviation of soil moisture constraints can lead to: (1) light becoming more limiting than water for photosynthesis, (2) greater stomatal conductance, which in turn leads to a greater dependence of leaf-level fluxes on atmospheric demand or (3) an increased capacity for transpiration, which can influence leaf temperature through evaporative cooling. To test this hypothesis, we conducted the same analysis during only the 10% wettest observations of mean soil moisture across all layers (Fig. 1b). During these periods, the correlation coefficient between GPP/ET and soil moisture was, as expected, reduced and in many cases was not statistically distinguishable from zero. However, the correlations between fluxes and atmospheric drivers during these periods were still generally smaller than the correlation between GPP and soil moisture calculated over the entire data record. Notably, the correlation between fluxes and VPD switched from negative during the entire data record to positive during the wettest conditions. This indicates that increased atmospheric demand during periods of low soil moisture limitation can increase diffusive gradients and drive greater ET[16], while also potentially providing a thermal environment conducive to higher rates of photosynthesis.

Ongoing debates centre around the role of atmospheric drivers versus soil moisture in driving ecosystem function, with a growing recognition of the importance of VPD in mediating vegetation activity[16,17]. We highlight here that VPD exerted a smaller role than soil moisture in driving daily variability in dryland fluxes and provide robust
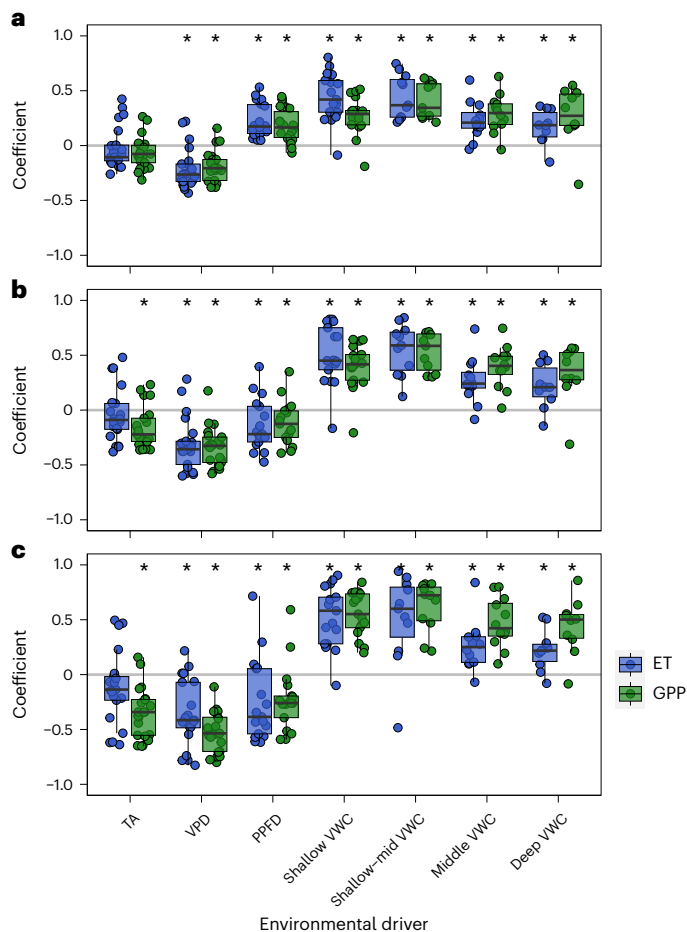
Fig. 2 | Correlation coefficients between GPP/ET and environmental drivers at half-hourly, weekly and monthly timescales. a–c, Correlation coefficients between GPP/ET and environmental drivers at half-hourly (**a**), weekly (**b**) and monthly (**c**) timescales. Environmental drivers include TA, VPD, PPFD and various layers of VWC (Methods provide the depths included in each layer). Asterisks indicate where coefficients are significantly different from zero ($\alpha = 0.05$). Box plot lines represent the interquartile range and median, whereas the whiskers represent 1.5 times the interquartile range.

Fig. 3 | Differences between hydrometeorological flux coefficients derived from remotely sensed versus EC approaches. a–f, Differences between coefficients derived from remotely sensed versus EC approaches (Δ coefficient) for atmospheric drivers (**a**,**b**) and soil moisture depths (**c–f**). Models used in this analysis include: FluxSat GPP, Global Land Evaporation Amsterdam Model (GLEAM) ET, Moderate Resolution Imaging Spectroradiometer (MODIS) GPP and ET, and Soil Moisture Active Passive (SMAP) L4C GPP. Values not significantly different from zero indicate the remotely sensed product replicates the EC-derived coefficient across sites. The presence of an asterisk indicates that Δ coefficient is significantly different from zero ($\alpha = 0.05$). Box plot lines represent the interquartile range and median, whereas the whiskers represent 1.5 times the interquartile range.

evidence of the important role of soil moisture for dryland GPP and ET over space and time. The importance of soil moisture at daily and half-hourly scales is quite notable, given that soil moisture dynamics generally tend to change much more slowly than fluctuations in VPD. Reasons for this could include: (1) dryland vegetation is highly adapted to rapidly respond to the fluctuations in soil water availability, given the frequently transient precipitation dynamics present in many xeric ecosystems[18,19] and (2) the seasonality of atmospheric aridity versus soil moisture is decoupled in some regions of the western United States due to monsoon-driven seasonality, whereby water availability frequently peaks in both the cooler springtime and the hotter late summer[14]. No matter the mechanism, the importance of soil water in drylands should elicit expanded monitoring of soil moisture and a greater recognition of the role that transient precipitation dynamics play for sustaining dryland ecosystem function, especially given observed and projected changes in the frequency, intensity and variability of precipitation with warming[20].

Remote sensing can capture the drivers of fluxes

Given the importance of capturing soil moisture sensitivity across the extensive dryland regions of the world and the relative paucity of EC towers in these biomes (especially outside of the United States), there is a pressing need for long-term and spatially extensive data sources that can
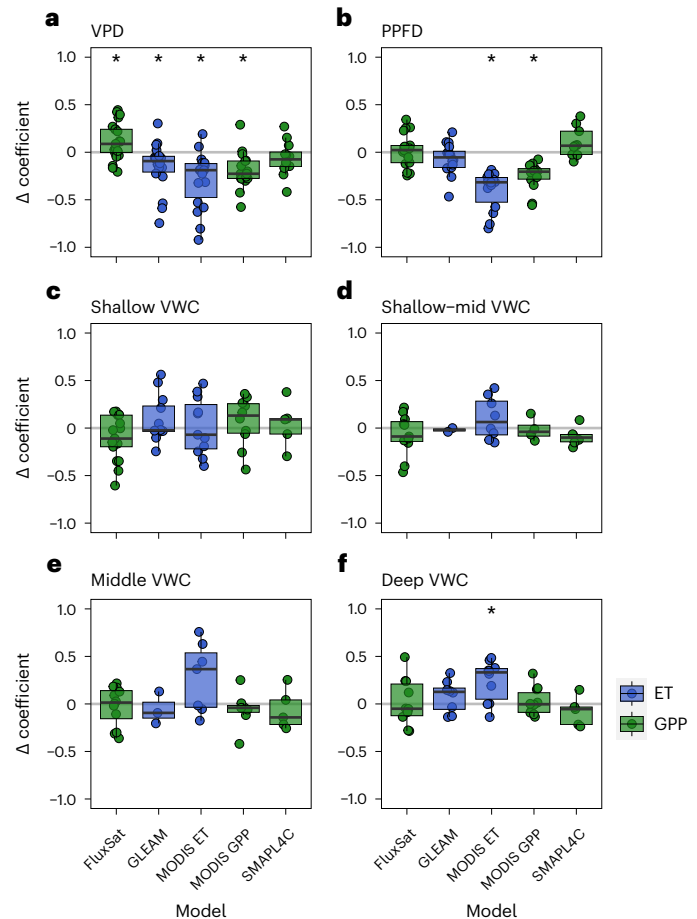
properly represent dryland ecosystem function. We therefore tested the ability of remotely sensed estimates of GPP and ET to accurately capture the sensitivity of drylands to various hydrometeorological drivers. We selected widely used GPP and ET products that span a range of methods (from purely empirical machine learning upscaling to semi-empirical models based on simplified process representations; Methods and Extended Data Table 2) and calculated their correlation coefficients with in situ meteorological measurements from the network of EC towers. These products generally replicated the eddy covariance-derived soil moisture coefficients (Fig. 3c–e and Extended Data Fig. 6c–e); in the aggregate, only the correlation between MODIS ET and deep soil moisture fluctuations was incorrectly represented (Fig. 3f and Extended Data Fig. 6f). Remotely sensed soil moisture coefficients were thus correlated with EC-derived coefficients (R^2 between 0.33 and 0.49) for all soil layers except the 10–20 cm layer (Extended Data Fig. 7).

Despite the ability of remotely sensed data to capture soil moisture correlation coefficients consistent with EC observations, they generally overpredicted the correlations between fluxes and atmospheric drivers (Fig. 3a,b), especially VPD. For example, the correlation coefficients

between remotely sensed GPP/ET products and VPD was on average 35% more negative than the VPD coefficient observed at flux tower sites (Extended Data Fig. 6a). As a result, the VPD coefficient for four out five flux products significantly deviated from EC coefficients (Fig. 3a), and the linkage between remotely sensed and EC coefficients was weak ($R^2 = 0.14$; Extended Data Fig. 7a,b). Two data products also showed sizeable negative relationships between PPFD and fluxes, whereas that coefficient tended to be around zero (or positive) when calculated using flux tower data (Fig. 1a, Fig. 3b and Extended Data Figs. 2 and 3). Given that the most consistent impact of climate change is increasing air temperature and thus increases in vapour pressure deficit, remotely sensed GPP and ET estimates that overrepresent the role of VPD could incorrectly capture ecosystem responses to climate change and climate extremes such as drought or heatwaves. Our results point to the need for satellite-based flux models to reconsider the role of atmospheric drivers in mediating dryland ecosystem fluxes, perhaps by directly incorporating information on soil moisture availability[21–23].

Despite some shortcomings representing the role of atmospheric drivers, these results highlight the striking ability of remote sensing approaches to capture the role of soil moisture in mediating dryland fluxes. These findings are particularly surprising considering that only GLEAM ET and SMAP L4C GPP directly include soil moisture constraints. This implies either: (1) that land surface greenness (the basis for optical remote sensing of vegetation function) is sufficiently coupled to soil moisture in drylands to correctly capture the sensitivity of carbon and water fluxes to soil moisture or (2) the coupling between soil moisture and VPD is strong enough that the simplified VPD scalars included in many of these data products can indirectly simulate flux sensitivity to soil moisture. However, with relatively few exceptions, the relationship between remotely sensed flux products and soil moisture is still largely indirect and thus developing products that can correctly capture in situ soil moisture dynamics is a pressing research need.

Given the success of the SMAP L4C GPP product in replicating EC-derived correlation coefficients, we next tested the ability of a SMAP-based soil moisture product[24] to capture daily fluctuations in surface and root-zone soil moisture. SMAP soil moisture estimates were indeed linked to in situ soil moisture measurements, though the R^2 between remotely sensed and in situ soil moisture decreased substantially with increasing soil depth, from 0.45 for surface soils to 0.13 at >50 cm depths (Extended Data Table 3). The correspondence between remotely sensed soil moisture and daily in situ soil moisture, combined with improvements in remotely sensed ET model performance when SMAP data are included[21,22], indicates that SMAP-based data products could be important tools to help constrain estimates of carbon–water cycling in land surface models through validation, benchmarking or data assimilation. In this regard, microwave remote sensing products show great promise for real-time monitoring of ecosystem function in arid and semiarid regions and for improving our understanding of how climate change (including the ongoing megadrought in the southwestern United States[25]) is impacting dryland ecosystems. However, given the large reliance of vegetation on deep soil moisture found here and elsewhere[26,27], more work needs to be done to develop and validate data products that can provide relevant information on deeper stores of plant-available water.

Land surface models underestimate soil moisture sensitivity

The tight coupling between soil moisture and ecosystem fluxes observed here could at least partly explain the poor performance of many land surface models in drylands, as properly representing soil moisture dynamics, along with vegetation responses to water stress, are frequently one of the largest modelling uncertainties[28–30]. Thus, we explored the degree to which a suite of land surface models from the Coupled Model Intercomparison Project Phase 6 (CMIP6; Methods) captured the sensitivity of GPP and ET to soil moisture in the flux tower network by calculating
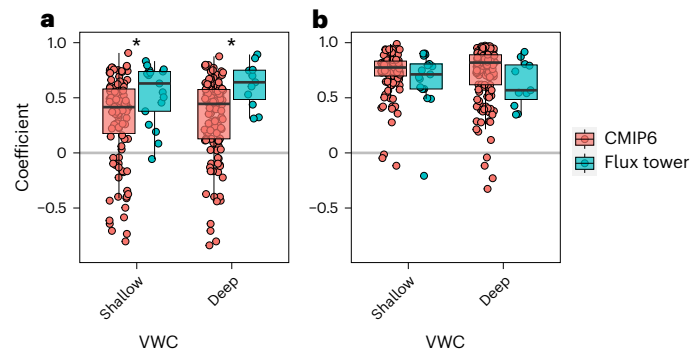

Fig. 4 | EC versus land surface model soil moisture correlation coefficients. Correlation coefficients between fluxes and shallow/deep soil moisture, as derived from flux tower data versus CMIP6 models. **a,b,** Correlation coefficients for GPP (**a**) and correlation coefficients for ET (**b**). Each point represents the Pearson's R between each environmental driver and flux, calculated over the growing season. Asterisks indicate where CMIP6 coefficients are significantly different than those from flux towers ($\alpha = 0.01$). Box plot lines represent the interquartile range and median, whereas the whiskers represent 1.5 times the interquartile range.

their correlation with shallow and deep soil moisture fluctuations. We found that models generally underestimated the correlation between GPP and shallow soil moisture by 42% and to deep soil moisture by 49% (Fig. 4a). This underestimation probably arose from: (1) challenges in modelling highly dynamic soil moisture fluctuations in biomes characterized by substantial belowground heterogeneity[28,29] and (2) error in the shape and slope of the 'beta functions' that downregulate modelled photosynthesis as a function of soil water availability, which are often poorly constrained or unconstrained by data[30]. Variability in CMIP6 correlation coefficients was also extremely large (spanning nearly the entire range of possible values), which was not reflected in the flux tower data. Negative relationships between GPP and soil moisture were also frequently predicted, though this directionality was largely absent in the flux tower data. Many (but not all) of these negative correlations were from the Canadian Earth System Model 5 (CanESM), which is known to have a reduced ability to accurately simulate dryland GPP compared with many other models[31]. Differences between CMIP6 and EC-derived soil moisture coefficients were still statistically different when this model was excluded from the ensemble, indicating that the inclusion of this model did not drive our conclusion that CMIP6 models underestimate the sensitivity of GPP to soil moisture.

In contrast, the soil moisture coefficients for ET in the CMIP6 models did not differ significantly from EC-derived values (Fig. 4b). However, given that the drastic underestimation of modelled GPP coefficients is also likely to indicate a lower coefficient for transpiration, this may indicate that the similarities between modelled and flux tower ET coefficients are driven by compensating errors (that is, an underestimation of transpiration sensitivity is offset by an overestimation of evaporation sensitivity). There are many uncertainties regarding partitioning ET into its constituent components[32], but future efforts to do so across dryland ecosystems could shed light on the discrepancies between how different models represent the sensitivity of ET to hydrometeorological drivers. Whereas the poor representation of soil moisture sensitivity in land surface models reflects shortcomings in our ability to simulate water-limited ecosystems, this finding also points to the value of ongoing modelling efforts towards better representing heterogeneous soil hydrology across depths[28] and the physiological responses of vegetation to water stress by mechanistically simulating plant hydraulics[33,34].

Soil moisture sensitivity in a changing climate

This Article provides compelling evidence that soil moisture is the primary driver of dryland carbon–water fluxes, though atmospheric drivers

(especially VPD) were important factors during infrequent wet periods. We found GPP was particularly responsive to deeper soil moisture pools, emphasizing their importance in sustaining dryland vegetation through dry and hot summer conditions[14,35,36]. Whereas recent increases in temperature and vapour pressure deficit are driving changes across many ecosystems, our results imply that the future functioning of drylands will be tied to local precipitation patterns, changes in snow accumulation and potential warming-enhanced depletion of soil moisture[10]. It is concerning, therefore, that drylands in the western United States have experienced drastic reductions in winter precipitation in recent decades, which is the source of moisture that primarily recharges deep soil layers[20,37,38]. The ramifications of deep soil moisture losses are severe and probably underpin many of the major plant mortality events observed across the region in recent years[39–42]. These decreases in water availability[43] might indicate US drylands are becoming more dependent on the inconsistent and transient fluctuations in shallow soil moisture that are derived from summer rainfall. A shift in the seasonality of water availability is an underappreciated dimension of climate change with consequences that remain to be evaluated[44].

In the face of ongoing climatic changes, our findings point to the need for an evolving understanding of dryland ecosystem function. Tools that properly represent the sensitivity of fluxes to both atmospheric drivers and soil moisture are essential to this process. We found that widely used land surface models (in their current iteration) seem unsuited for this task, though advances in modelling soil hydrology and vegetation hydraulics are potentially promising in this regard. Although previous model-based analyses have found that soil moisture plays a critical role in mediating global carbon uptake[45], our results suggest that these models may still be underestimating how important soil water is for vegetation function. This underestimation becomes even more critical given projections of increasing drought frequency and intensity in drylands[46]. Although land surface models fell short in quantifying the sensitivity of GPP to soil moisture, remote sensing products generally succeeded, despite the large mismatch in spatial scale between satellite data products and flux towers. This result was also surprising considering the inherent challenges in measuring ecosystems from satellites in biomes that are characterized by large day-to-day variability in ecosystem fluxes (that is, 'hot moments'[13]). Data products derived from microwave remote sensing, in particular, seem very promising for generating accurate estimates of ecosystem fluxes and shallow soil moisture. However, the finding that remote-sensing approaches tend to overestimate the sensitivity of fluxes to atmospheric drivers poses a challenge for properly representing dryland ecosystem dynamics in an aridifying climate.

Ultimately, our findings highlight the importance of long-term in situ monitoring of dryland ecosystem fluxes and soil moisture. Committing resources to this area will be crucial to validate the newest generation of remote sensing products and land surface models that include a more physiologically informed view of how carbon and water flows through drylands. Such advances will set the stage for an improved understanding of water-limited biomes in the face of climate change and improve the accuracy of near-term ecological drought monitoring.

Online content

Any methods, additional references, Nature Portfolio reporting summaries, source data, extended data, supplementary information, acknowledgements, peer review information; details of author contributions and competing interests; and statements of data and code availability are available at https://doi.org/10.1038/s41561-023-01351-8.

References

1. Ahlstrom, A. et al. The dominant role of semi-arid ecosystems in the tren and variability of the land CO_2 sink. *Science* **348**, 4503–4518 (2015).
2. Poulter, B. et al. Contribution of semi-arid ecosystems to interannual variability of the global carbon cycle. *Nature* **509**, 600–603 (2014).
3. Zhou, L., Chen, H. & Dai, Y. Stronger warming amplification over drier ecoregions observed since 1979. *Environ. Res. Lett.* **10**, 064012 (2015).
4. Cook, B. I., Ault, T. R. & Smerdon, J. E. Unprecedented 21st century drought risk in the American Southwest and Central Plains. *Sci. Adv.* **1**, e1400082 (2015).
5. Cook, B. et al. Uncertainties, limits, and benefits of climate change mitigation for soil moisture drought in southwestern North America. *Earth's Future* **9**, e2021EF002014 (2021).
6. Barnes, M. L. et al. Improved dryland carbon flux predictions with explicit consideration of water–carbon coupling. *Commun. Earth Environ.* **2**, 248 (2021).
7. MacBean, N. et al. Dynamic global vegetation models underestimate net CO_2 flux mean and inter-annual variability in dryland ecosystems. *Environ. Res. Lett.* **16**, 094023 (2021).
8. Smith, W. K. et al. Remote sensing of dryland ecosystem structure and function: progress, challenges, and opportunities. *Remote Sens. Environ.* **233**, 111401 (2019).
9. Ficklin, D. L. & Novick, K. A. Historic and projected changes in vapor pressure deficit suggest a continental-scale drying of the United States atmosphere. *J. Geophys. Res.* **122**, 2061–2079 (2017).
10. Cook, B. et al. Twenty-first century drought projections in the CMIP6 forcing scenarios. *Earth's Future* **8**, e2019EF001461 (2020).
11. Lian, X. et al. Multifaceted characteristics of dryland aridity changes in a warming world. *Nat. Rev. Earth Environ.* **2**, 232–250 (2021).
12. Thompson, S. E. et al. Comparative hydrology across AmeriFlux sites: the variable roles of climate, vegetation, and groundwater. *Water Resour. Res.* **47**, 1–17 (2011).
13. Kannenberg, S. A., Bowling, D. R. & Anderegg, W. R. L. Hot moments in ecosystem fluxes: high GPP anomalies exert outsized influence on the carbon cycle and are differentially driven by moisture availability across biomes. *Environ. Res. Lett.* **15**, 054004 (2020).
14. Kannenberg, S. A. et al. Quantifying the drivers of ecosystem fluxes and water potential across the soil–plant–atmosphere continuum in an arid woodland. *Agric. For. Meteorol.* **329**, 109269 (2023).
15. Sun, X., Wilcox, B. P. & Zou, C. B. Evapotranspiration partitioning in dryland ecosystems: a global meta-analysis of in situ studies. *J. Hydrol.* **576**, 123–136 (2019).
16. Novick, K. A. et al. The increasing importance of atmospheric demand for ecosystem water and carbon fluxes. *Nat. Clim. Change* **6**, 1023–1027 (2016).
17. Grossiord, C. et al. Plant responses to rising vapor pressure deficit. *N. Phytol.* **226**, 1550–1566 (2020).
18. Huxman, T. E. et al. Precipitation pulses and carbon fluxes in semiarid and arid ecosystems. *Oecologia* **141**, 254–268 (2004).
19. Schwinning, S. & Sala, O. E. Hierarchy of responses to resource pulses in arid and semi-arid ecosystems. *Oecologia* **141**, 211–220 (2004).
20. Zhang, F. et al. Five decades of observed daily precipitation reveal longer and more variable drought events across much of the western United States. *Geophys. Res. Lett.* **48**, 1–11 (2021).
21. Brust, C. et al. Using SMAP Level-4 soil moisture to constrain MOD16 evapotranspiration over the contiguous USA. *Remote Sens. Environ.* **255**, 112277 (2021).
22. Purdy, A. J. et al. SMAP soil moisture improves global evapotranspiration. *Remote Sens. Environ.* **219**, 1–14 (2018).
23. Stocker, B. D. et al. Quantifying soil moisture impacts on light use efficiency across biomes. *N. Phytol.* **218**, 1430–1449 (2018).

24. Mladenova, I. E., Bolten, J. D., Crow, W., Sazib, N. & Reynolds, C. Agricultural drought monitoring via the assimilation of SMAP soil moisture retrievals into a global soil water balance model. *Front. Big Data* **3**, 10 (2020).

25. Williams, A. P., Cook, B. I. & Smerdon, J. E. Rapid intensification of the emerging southwestern North American megadrought in 2020–2021. *Nat. Clim. Change* **12**, 232–234 (2022).

26. Miguez-Macho, G. & Fan, Y. Spatiotemporal origin of soil water taken up by vegetation. *Nature* **598**, 624–628 (2021).

27. McCormick, E. L. et al. Widespread woody plant use of water stored in bedrock. *Nature* **597**, 225–229 (2021).

28. MacBean, N. et al. Testing water fluxes and storage from two hydrology configurations within the ORCHIDEE land surface model across US semi-arid sites. *Hydrol. Earth Syst. Sci.* **24**, 5203–5230 (2020).

29. Qiao, L., Zuo, Z. & Xiao, D. Evaluation of soil moisture in CMIP6 simulations. *J. Clim.* **35**, 779–800 (2022).

30. Trugman, A. T., Medvigy, D., Mankin, J. S. & Anderegg, W. R. L. Soil moisture stress as a major driver of carbon cycle uncertainty. *Geophys. Res. Lett.* **45**, 6495–6503 (2018).

31. Collier, N. et al. The International Land Model Benchmarking (ILAMB) system: design, theory, and implementation. *J. Adv. Model. Earth Syst.* **10**, 2731–2754 (2018).

32. Stoy, P. C. et al. Reviews and syntheses: turning the challenges of partitioning ecosystem evaporation and transpiration into opportunities. *Biogeosciences* **16**, 3747–3775 (2019).

33. Kennedy, D. et al. Implementing plant hydraulics in the Community Land Model, version 5. *J. Adv. Model. Earth Syst.* **11**, 485–513 (2019).

34. Sperry, J. S. et al. Predicting stomatal responses to the environment from the optimization of photosynthetic gain and hydraulic cost. *Plant Cell Environ.* **40**, 816–830 (2017).

35. Samuels-Crow, K. E., Ogle, K. & Litvak, M. E. Atmosphere–soil interactions govern ecosystem flux sensitivity to environmental conditions in semiarid woody ecosystems over varying timescales. *J. Geophys. Res. Biogeosci.* **125**, 1–16 (2020).

36. Ripullone, F., Camarero, J. J., Colangelo, M. & Voltas, J. Variation in the access to deep soil water pools explains tree-to-tree differences in drought-triggered dieback of Mediterranean oaks. *Tree Physiol.* **40**, 591–604 (2020).

37. Mote, P. W., Li, S., Lettenmaier, D. P., Xiao, M. & Engel, R. Dramatic declines in snowpack in the western US. *npj Clim. Atmos. Sci.* **1**, 2 (2018).

38. Siirila-Woodburn, E. et al. A low-to-no snow future and its impacts on water resources in the western United States. *Nat. Rev. Earth Environ.* **2**, 800–819 (2021).

39. Breshears, D. D. et al. Regional vegetation die-off in response to global-change-type drought. *Proc. Natl Acad. Sci. USA* **102**, 15144–15148 (2005).

40. Kannenberg, S. A., Driscoll, A. W., Malesky, D. & Anderegg, W. R. L. Rapid and surprising dieback of Utah juniper in the southwestern USA due to acute drought stress. *For. Ecol. Manag.* **480**, 118639 (2021).

41. Ganey, J. L. & Vojta, S. C. Tree mortality in drought-stressed mixed-conifer and ponderosa pine forests, Arizona, USA. *For. Ecol. Manag.* **261**, 162–168 (2011).

42. Hantson, S., Huxman, T. E., Kimball, S., Randerson, J. T. & Goulden, M. L. Warming as a driver of vegetation loss in the Sonoran Desert of California. *J. Geophys. Res. Biogeosci.* **126**, 285–295 (2021).

43. Lal, P., Shekhar, A., Gharun, M. & Das, N. N. Spatiotemporal evolution of global long-term patterns of soil moisture. *Sci. Total Environ.* **867**, 161470 (2023).

44. Hajek, O. L. & Knapp, A. K. Shifting seasonal patterns of water availability: ecosystem responses to an unappreciated dimension of climate change. *N. Phytol.* **233**, 119–125 (2022).

45. Green, J. K. et al. Large influence of soil moisture variability on long-term terrestrial carbon uptake. *Nature* **565**, 476–479 (2019).

46. Li, H. et al. Drylands face potential threat of robust drought in the CMIP6 SSPs scenarios. *Environ. Res. Lett.* **16**, 114004 (2021).

Methods

Site selection and flux data processing

To characterize the sensitivity of ecosystem fluxes to hydrometeorological drivers, we synthesized data from all AmeriFlux towers in the western United States with at least four years of data, an aridity index (the ratio of mean annual precipitation to potential evapotranspiration) of <0.65, <500 mm mean annual precipitation and no active management or manipulation (Fig. 1 and Extended Data Table 1). All sites except one (US-Rls) had a mean aridity index of less than 0.5. Our sites were constrained to the western United States due to the paucity of dryland flux towers that meet our criteria in other regions. However, these sites represent a wide diversity of climates, topographies and vegetation types and are thus relevant for understanding dryland functioning globally. Atmospheric drivers—photosynthetic photon flux density (PPFD), air temperature (TA) and vapour pressure deficit (VPD)—were measured at most sites, as were measurements of soil volumetric water content (VWC) of at least one depth. VPD was derived from relative humidity and TA when not provided. The depths of soil moisture measurements were attained from site principal investigators. When not directly measured, PPFD was considered to be proportional to incoming shortwave radiation[47]. To compare soil moisture dynamics across sites, soil volumetric water content measurements were binned (averaged) into four depths at each site, when present: a 'shallow' layer from 0 to ≤10 cm, a 'shallow–mid' layer from >10 to ≤20 cm, a 'middle' layer from >20 to ≤50 cm, and a 'deep' layer consisting of measurements >50 cm.

Net ecosystem exchange, TA, PPFD and VPD were gap-filled using a look-up table approach and net ecosystem exchange was partitioned into GPP and ecosystem respiration using the nighttime partitioning method[48], as implemented in the R package REddyProc[49]. Evapotranspiration (ET) was calculated by dividing the latent heat flux by the latent heat of vapourization. Because our goal was to quantify the drivers of vegetation activity, we then limited our dataset to daytime observations during the growing season. We defined start and end of the growing season of each site-year using smoothed curves of GPP[13,50]. First, at each site, winter was defined as the time before day of year 70 and after day of year 330. Next, for each site-year we constructed smoothed curves of seasonal GPP and daily curves of incoming shortwave radiation using the *loess* function in R with a span of 0.5. The start of the growing season was considered to be the first time point at which this curve crossed a threshold of mean winter GPP + 30% of the maximum smoothed GPP amplitude, and the end of the growing season was considered to be the last time point when it fell below this threshold. Start- and end-of-season dates were then averaged for each site. For weekly and monthly analyses, growing seasons were defined as the next week or month following the start date until the week or month before the end date. Daytime was defined as 9 a.m. to 5 p.m. at each site, based on the mean diurnal cycle of solar radiation. All daytime and growing season flux and meteorological data were then summed (fluxes) or averaged (all other variables) to the daily timescale.

Remotely sensed data products

We next compared the sensitivity of EC fluxes to several common satellite-based GPP and ET models. To do so, we amassed five different data products that operate at fast temporal scales (eight days or less) and span a wide range of methods (Extended Data Table 2[51–55]). We used two GPP products—the gap-filled MODIS product (MOD17A2GF[51]) and the SMAP Level 4 Carbon (L4C) product[52]—that are based on light-use efficiency theory, in which GPP is proportional to absorbed photosynthetically active radiation. In both products, a biome-specific 'optimal' light-use efficiency is down-regulated under non-optimal temperature and/or moisture conditions. The MODIS GPP model down-regulates GPP under both low minimum temperatures and high VPD, whereas the SMAP GPP model also includes responses to low root zone (0–100 cm) soil moisture and frozen ground. As a complement to these semi-empirical GPP products, we also use the empirical

FluxSat GPP product[53], which upscales global eddy covariance GPP estimates with a neural network based on MODIS multispectral surface reflectance and top-of-atmosphere radiation. For ET, we used two products based on physical evapotranspiration models: the gap-filled Penman–Monteith-based MODIS product (MOD16A2GF[54]) and the Priestley–Taylor-based GLEAM product[55]. In both cases, potential evapotranspiration from the physical models is reduced under moisture stress, which is defined based on VPD in the MODIS model and based on vegetation optical depth and root-zone soil moisture (from a multi-layer water balance model) in the GLEAM model. For these data products, we extracted the grid cell that contained the flux towers for all analyses.

To assess the degree to which in situ soil moisture dynamics can be remotely sensed, we also obtained surface and root-zone soil moisture data for each flux tower site from the L-band microwave Enhanced SMAP dataset[24]. Remotely sensed soil moisture estimates were smoothed from 3-day to a daily timescale to be directly comparable with flux tower data using a *loess* smoothing spline with a span of 0.05. These data were then constrained to the same growing seasons and years as the flux tower data. The error in remotely sensed soil moisture correlation coefficients (Δ coefficient) was quantified as the soil moisture coefficient derived from remotely sensed data products minus the EC-derived coefficient.

CMIP6 model output

We extracted monthly GPP, ET and soil moisture data from the grid cell corresponding to our flux tower locations from a single ensemble member (r1i1p1f1) for a suite of 11 CMIP6 land surface models: ACCESS-ESM1-5, BCC-CSM2-MR, CanESM5, CESM2-WACCM, CMCC-CM2-SR5, MPI-ESM1-2-LR, NorESM2-LM, NorESM2-MM, TaiESM1, E3SM-1-0 and MIROC6. For consistency with EC-derived measurements and microwave remote sensing products described below, we extracted the top 10 cm and the 1 m soil moisture variables. The 10 cm CMIP6 soil moisture product is analogous to the 'shallow' in situ soil layer, whereas the 1 m soil moisture product is analogous to the 'deep' in situ soil layer. CMIP6 output extends only through the year 2014 whereas the EC data have variable dataset lengths. To maximize the comparability between EC and model-derived fluxes, we constrained the two datasets to the same time periods for this analysis. Differences in the spatial and temporal scales at which eddy covariance, remotely sensed and CMIP6 data operate could introduce noise into direct comparisons among them. Such mismatches in scale have the potential to 'smooth out' point-scale variability, potentially leading to an apparent underestimation of variability. Regardless of whether this underestimation is due to spatial scaling or issues inherent to the coarser-scale data, it remains a critical concern. Comparisons between these products are essential for evaluating sensitivity across different data products and spatio-temporal scales, especially given the widespread use of land surface models for prediction.

Statistical analyses

The sensitivity of carbon and water fluxes to various meteorological drivers was calculated as the Pearson's *R* of the relationship between a given flux and hydrometeorological driver. Pearson's *R* is indicative of the slope of the relationship between two standardized variables and is thus reflective of how strongly a flux responds to an environmental driver. The sign of the coefficient reflects the direction of the relationship, where a larger value (either positive or negative) indicates that a given flux responds more strongly to variability in a given variable. A coefficient near zero indicates that the flux was not responsive to a given variable. The relationship between hydrometeorological drivers and fluxes, though frequently linear in nature, can also take on a wide variety of functional forms. Therefore, we also computed the Spearman's correlation coefficient, which does not assume linearity and instead assesses the strength of the relationship between two variables using a monotonic function.

To quantify the influence of hydrometeorological drivers on GPP and ET while accounting for any predictor collinearity, we additionally performed a relative weight analysis (RWA)[56] using the R package rwa (cran.r-project.org/web/packages/rwa/rwa.pdf). RWA partitions the explained variance across multiple predictors by transforming correlated predictors into orthogonal variables, performing a linear model on the transformed variables and then transforming the resulting coefficients back to the original metric. The resulting relative weights are only comparable across sites if the underlying model structure is the same (that is, contains the same predictor variables), which is not the case across our sites. Therefore, we conducted RWA only on the sites that contained the predictors that were most commonly available (TA, VPD, PPFD, shallow soil moisture and shallow–mid soil moisture).

We used ordinary least squares regression to compare correlation coefficients quantified across different data sources and to compare microwave remote sensing soil moisture products to in situ soil moisture, after assessing the normality and heteroscedasticity of model residuals. Two-tailed t tests were used to assess differences between soil moisture coefficients across data products and to test if a coefficient was significantly different from zero. All analyses were conducted in R 4.2.2.2[57].

Data availability

All data used for our analyses are publicly available. Eddy covariance tower data are available at ameriflux.lbl.gov, CMIP6 model output are accessible from esgf-node.llnl.gov/search/cmip6/. SMAP L4C, MOD16 and MOD17 data were all obtained using the AppEEARS subsetting tool (https://appeears.earthdatacloud.nasa.gov/). FluxSat data were obtained from the Oak Ridge National Lab Distributed Active Archive Center (https://daac.ornl.gov/VEGETATION/guides/FluxSat_GPP_FPAR.html), and GLEAM data were obtained from https://www.gleam.eu/.

References

47. Britton, C. & Dodd, J. Relationships of photosynthetically active radiation and shortwave irradiance. *Agric. Meteorol.* **17**, 1–7 (1976).
48. Reichstein, M. et al. On the separation of net ecosystem exchange into assimilation and ecosystem respiration: review and improved algorithm. *Glob. Change Biol.* **11**, 1424–1439 (2005).
49. Wutzler, T. et al. Basic and extensible post-processing of eddy covariance flux data with REddyProc. *Biogeosciences* **15**, 5015–5030 (2018).
50. Keenan, T. F. et al. Net carbon uptake has increased through warming-induced changes in temperate forest phenology. *Nat. Clim. Change* **4**, 598–604 (2014).
51. Running, S. W. et al. A continuous satellite-derived measure of global terrestrial primary production. *BioScience* **54**, 547 (2004).
52. Jones, L. A. et al. The SMAP level 4 carbon product for monitoring ecosystem land–atmosphere CO_2 exchange. *IEEE Trans. Geosci. Remote Sens.* **55**, 6517–6532 (2017).
53. Joiner, J. & Yoshida, Y. Global MODIS and FLUXNET-derived daily gross primary production, V2. *ORNL DAAC* https://doi.org/10.3334/ORNLDAAC/1835 (2021).
54. Mu, Q., Zhao, M. & Running, S. W. Improvements to a MODIS global terrestrial evapotranspiration algorithm. *Remote Sens. Environ.* **115**, 1781–1800 (2011).
55. Martens, B. et al. GLEAM v3: satellite-based land evaporation and root-zone soil moisture. *Geosci. Model Dev.* **10**, 1903–1925 (2017).
56. Tonidandel, S. & LeBreton, J. M. Relative importance analysis: a useful supplement to regression analysis. *J. Bus. Psychol.* **26**, 1–9 (2011).
57. R Core Team *R: A Language and Environment for Statistical Computing* (R Foundation for Statistical Computing, 2022).

Acknowledgements

Author contributions

S.A.K. initially conceived of the research, with subsequent contributions from all authors. W.R.L.A., M.L.B. and M.P.D. assisted with data extraction. S.A.K. performed all data analysis and wrote the first draft of the manuscript. All authors contributed to subsequent manuscript revisions.

Competing interests

The authors declare no competing interests.

Additional information

Extended data is available for this paper at https://doi.org/10.1038/s41561-023-01351-8.

Supplementary information The online version contains supplementary material available at https://doi.org/10.1038/s41561-023-01351-8.

Correspondence and requests for materials should be addressed to Steven A. Kannenberg.

Peer review information *Nature Geoscience* thanks Stefan Hagemann, Andrew F. Feldman and the other, anonymous, reviewer(s) for their contribution to the peer review of this work. Primary Handling Editors: Alireza Bahadori, Xujia Jiang, in collaboration with the *Nature Geoscience* team.

Reprints and permissions information is available at www.nature.com/reprints.
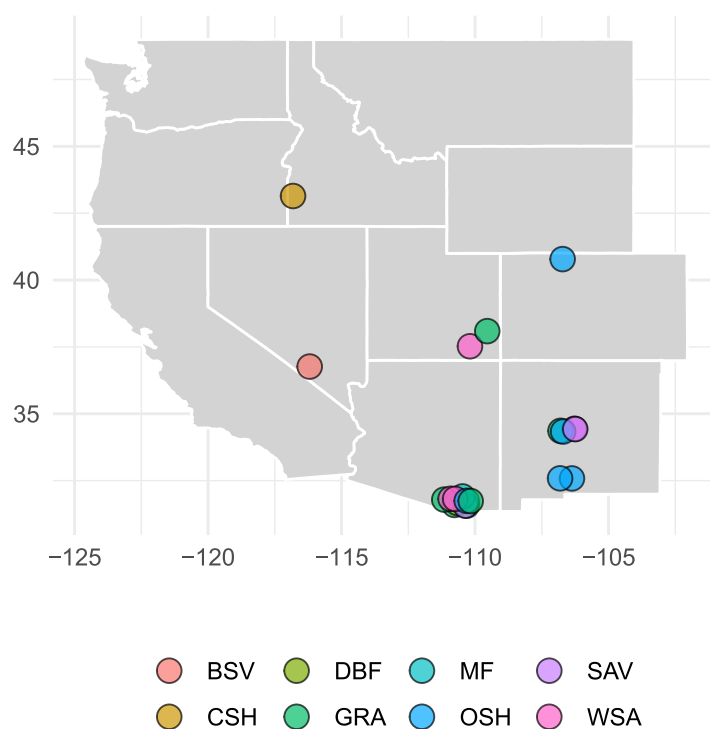
Extended Data Fig. 1 | Map of the eddy covariance tower sites used in this analysis. Color corresponds to the IGBP vegetation type.

	TA	VPD	PPFD	Shallow VWC	Shallow–mid VWC	Middle VWC	Deep VWC
ADR	−0.19	−0.32	−0.12	0.33			
Ses	−0.13	−0.21	−0.04				
Seg	n.s.	−0.15	n.s.				
Jo1	−0.18	−0.06		0.22	0.3	0.42	
Jo2	−0.22	−0.23	n.s.	0.09	0.41	0.33	
SRC	−0.09	−0.39		0.54	0.65		
CdM	−0.24	−0.11	0.18	0.4	0.72	0.6	0.63
Whs	−0.26	−0.43	−0.15	0.39		0.13	
CMW	0.18	−0.18		0.38	0.36	0.37	0.26
Cop	−0.24	−0.26		0.29	0.36	0.41	0.57
LS1	0.29	n.s.	n.s.	0.39		0.46	0.42
LS2	0.19	−0.11	0.1	0.32		0.45	0.28
Wjs	−0.07	−0.24	−0.04				
Wkg	−0.19	−0.37	−0.09	0.58	0.59	0.21	
Rls	n.s.	−0.16	0.24	0.21			0.17
SRM	−0.24	−0.44	−0.22	0.55	0.62	0.7	0.48
SRS	−0.11	−0.28	−0.12	0.34	0.36	0.35	0.25
Mpj	−0.33	−0.39	−0.06				
Aud	n.s.	−0.29	0.06	0.5	0.31		
SRG	−0.2	−0.39	−0.16	n.s.	0.67		0.52
Wdn	0.36	0.32	0.32	−0.28		n.s.	
Mean	−0.08	−0.22	−0.01	0.33	0.49	0.36	0.40

Extended Data Fig. 2 | See next page for caption.

Extended Data Fig. 2 | Correlation plot representing the coefficient of daily GPP to various environmental drivers. Each row represents a different flux tower site, while the last row represents the mean across sites. Sites are arranged (top to bottom) in order of decreasing aridity (mean climatic water deficit). Color, point size, and number indicates the Pearson's R correlation coefficient. Missing values indicate a lack of data for that particular variable. 'n.s.' indicates a non-significant relationship ($\alpha = 0.05$). Deep VWC correlations for US-Whs were excluded due to their limited temporal record.
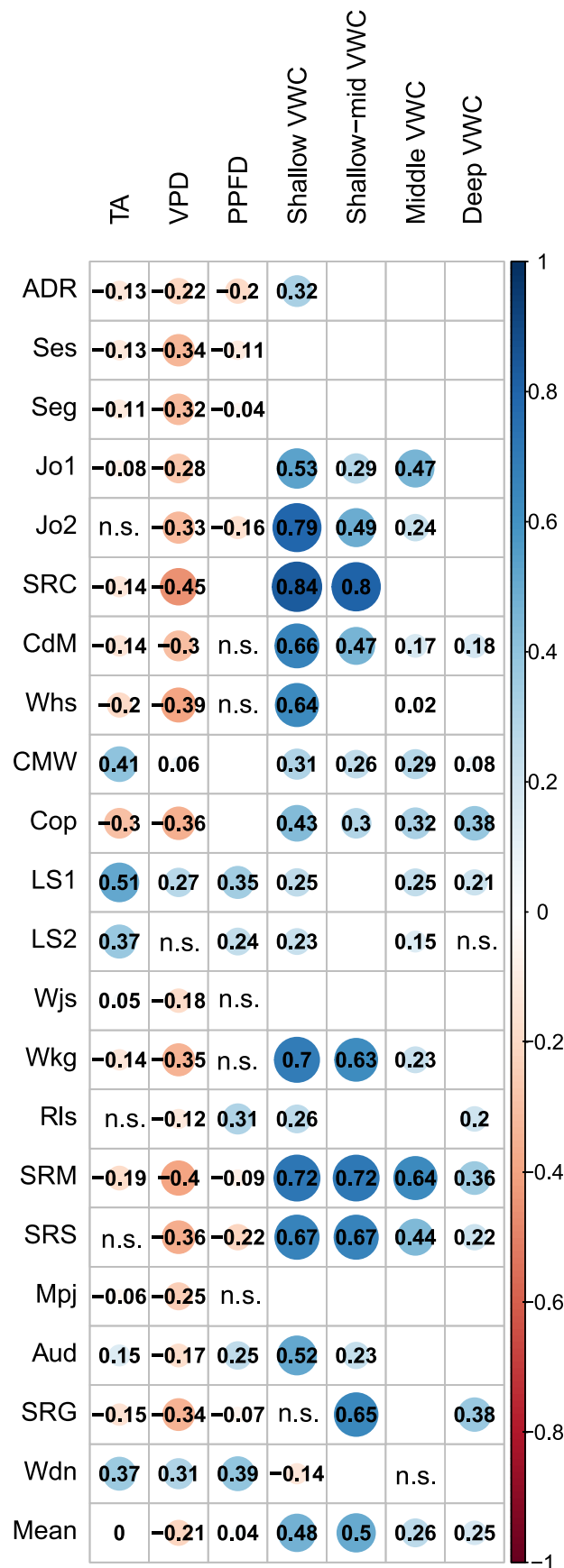
Extended Data Fig. 3 | See next page for caption.

Extended Data Fig. 3 | Correlation plot representing the coefficient of daily ET to various environmental drivers. Each row represents a different flux tower site, while the last row represents the mean across sites. Sites are arranged (top to bottom) in order of decreasing aridity (mean climatic water deficit). Color, point size, and number indicates the Pearson's R correlation coefficient. Missing values indicate a lack of data for that variable. 'n.s.' indicates a non-significant relationship ($\alpha = 0.05$). Deep VWC correlations for US-Whs were excluded due to their limited temporal record.
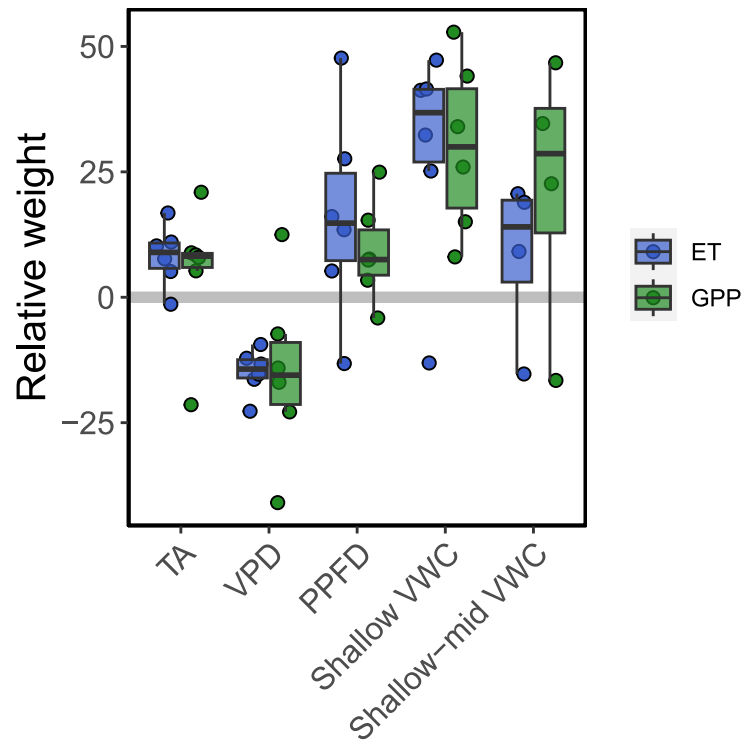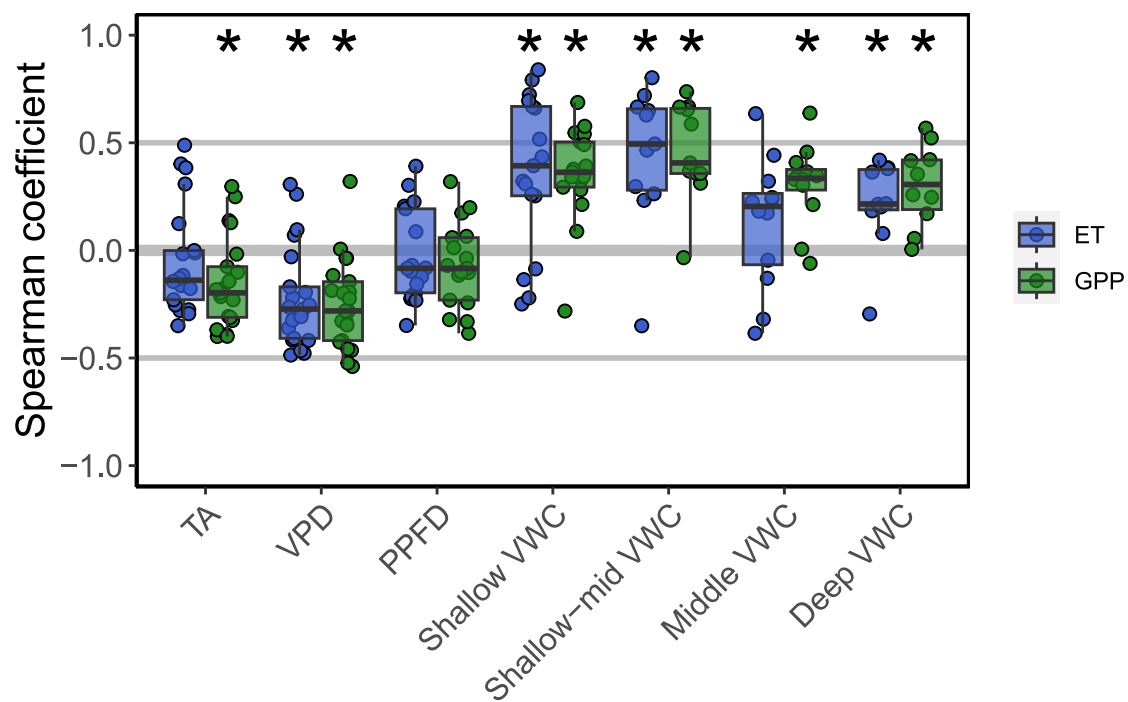
Extended Data Fig. 4 | Relative weights for models between GPP/ET and hydrometeorological drivers. Only a subset of sites were used for this analysis in order to keep relative weights comparable (see Methods). Box plot lines represent the interquartile range and median, while the whiskers represent 1.5 times the interquartile range.

Extended Data Fig. 5 | Spearman's correlation coefficients between daily GPP/ET and environmental drivers. Environmental drivers include air temperature (TA), vapor pressure deficit (VPD), photosynthetic photon flux density (PPFD), and various layers of volumetric water content (VWC, see Methods for the depths included in each layer). Asterisks indicate where coefficients are significantly different from zero ($\alpha = 0.05$). Box plot lines represent the interquartile range and median, while the whiskers represent 1.5 times the interquartile range.
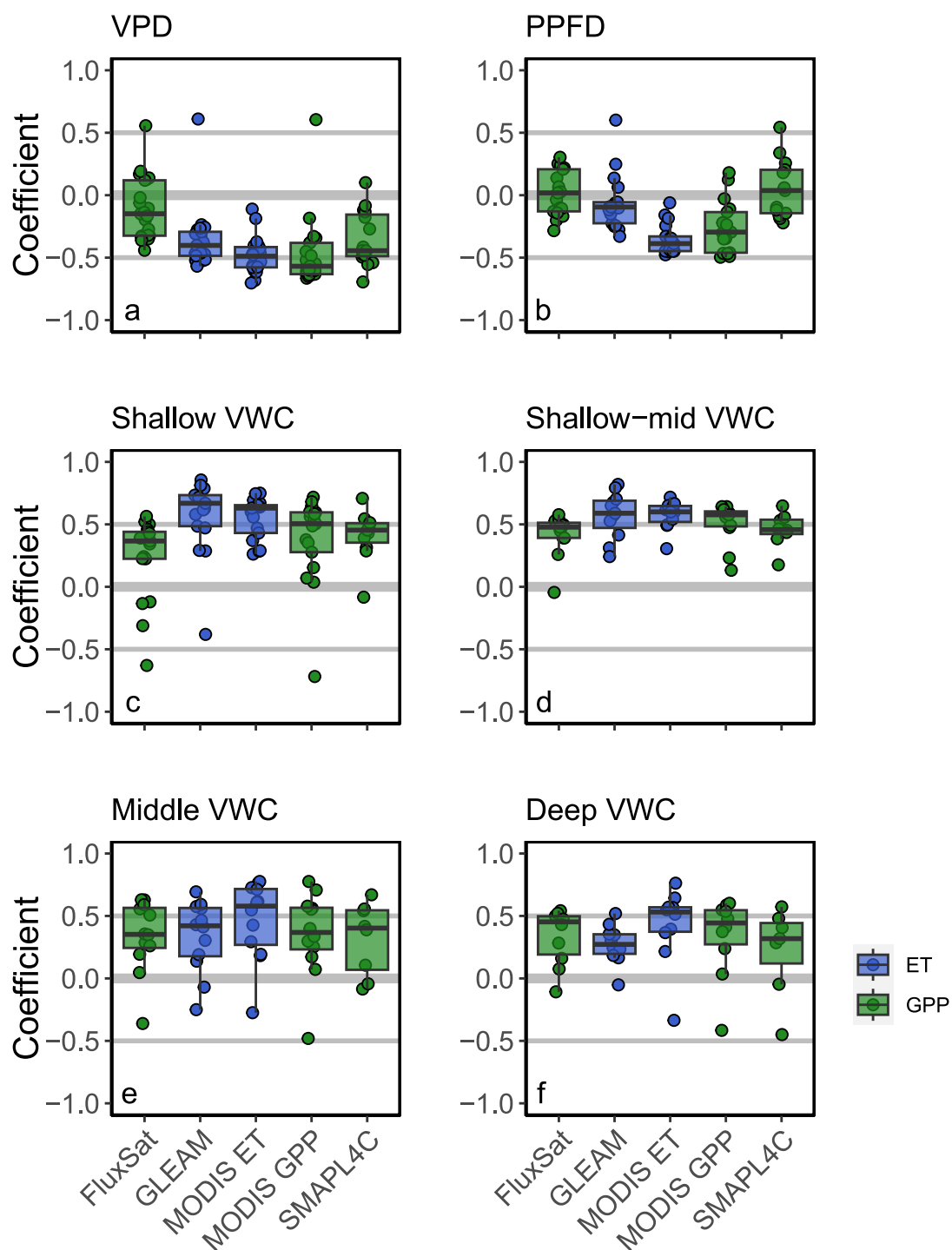
Extended Data Fig. 6 | Remotely-sensed correlation coefficients. Pearsons' R coefficient between various data products (boxplots and points) and a given environmental driver (panels) at each site. Box plot lines represent the interquartile range and median, while the whiskers represent 1.5 times the interquartile range.

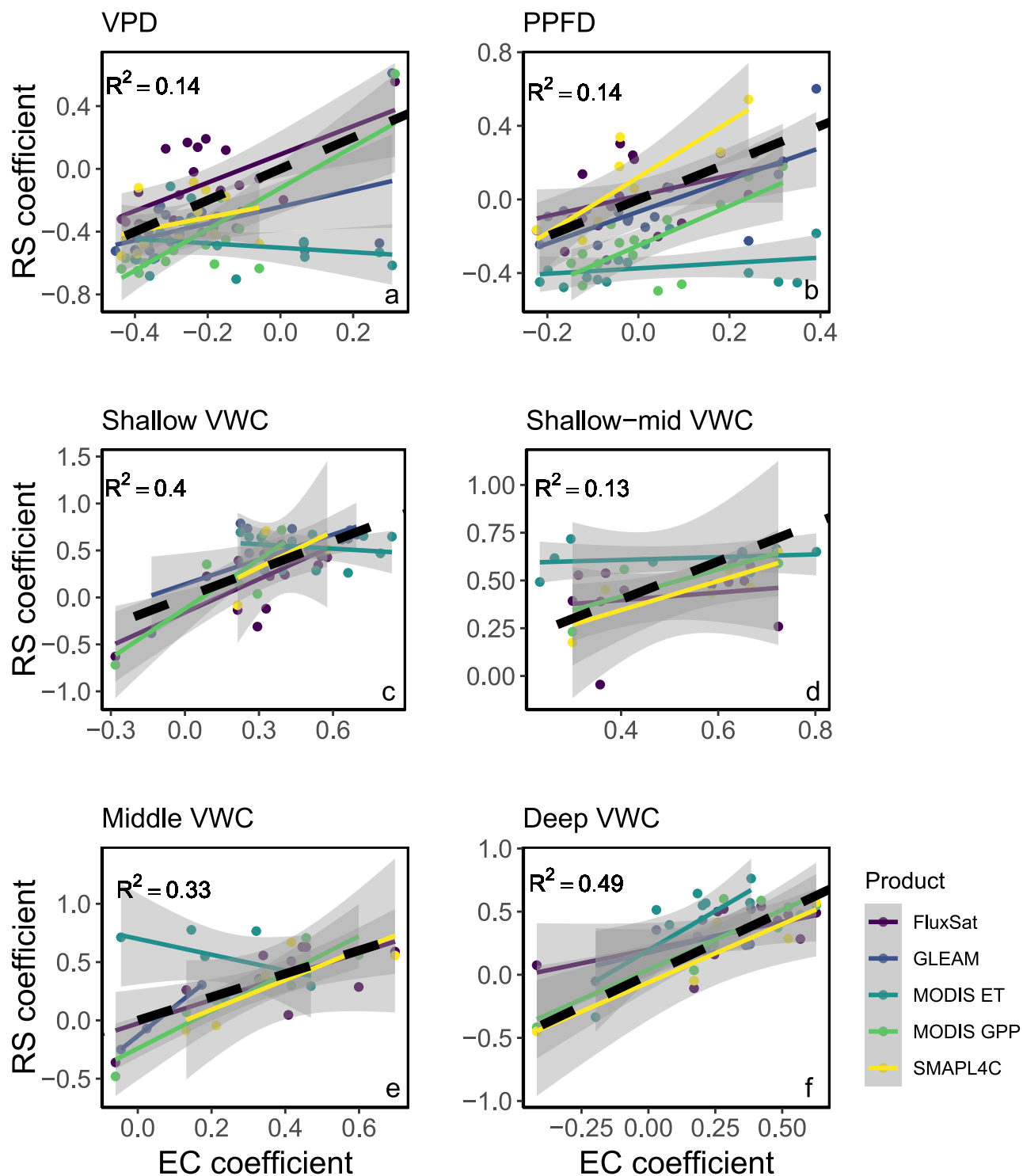**Extended Data Fig. 7 | Eddy covariance (EC) versus remotely-sensed (RS) coefficients for various environmental drivers.** R^2 values are those from a linear model containing all remotely-sensed data products (all models statistically significant at $\alpha = 0.05$), and the dashed black lines are 1:1 lines. Gray shading indicates the 95% confidence interval.

Extended Data Table 1 | Basic site information for all eddy covariance towers

Site ID	Latitude	Longitude	Elevation (m)	MAT (˚C)	MAP (mm)	Vegetation type	Climate	Data present	DOI
ADR	36.7653	-116.6933	842	17.5	110	BSV	Bwh	2011-2017	10.17190/AMF/1418680
Aud	31.5907	-110.5104	1469	14.85	438.35	GRA	Bsk	2002-2011	10.17190/AMF/1246028
CdM	37.52414	-109.74714	1860	11.3	348	WSA	Bsk	2019-2021	10.17190/AMF/1865477
CMW	31.663654	-110.177692	1199	17	288	DBF	Bsh	2000-2019	10.17190/AMF/1660339
Cop	38.09	-109.39	1520	9.67	323.088	GRA	Bsk	2001-2007	10.17190/AMF/1246129
Jo1	32.582	-106.635	1188	14.7	245.1	OSH	Bwk	2010-2019	10.17190/AMF/1767833
Jo2	32.5849	-106.6032	1469	17.5	282.3	OSH	Bwk	2010-2019	10.17190/AMF/1617696
LS1	31.56153	-110.14033	1230	17	288	GRA	Bwh	2002-2007	10.17190/AMF/1660346
LS2	31.565916	-110.134403	1240	17	288	SAV	Bwh	2002-2007	10.17190/AMF/1660347
Mpj	34.4385	-106.2377	2196	10.5	385	WSA	Bsk	2008-2021	10.17190/AMF/1246123
Rls	43.1439	-116.7356	1608	8.4	333	CSH	Bsh	2014-2018	10.17190/AMF/1418682
Seg	34.3623	-106.702	1596	13.667	273.304	GRA	Bsk	2007-2021	10.17190/AMF/1246124
Ses	34.3349	-106.7442	1604	13.722	275.082	OSH	Bsk	2007-2021	10.17190/AMF/1246125
SRC	31.9083	-110.8395	950	22	330	MF	Bwh	2008-2014	10.17190/AMF/1246127
SRG	31.789379	-110.827675	1291	17	420	GRA	Bsk	2008-2020	10.17190/AMF/1246154
SRM	31.8214	-110.8661	1120	17.92	380	WSA	Bsk	2003-2020	10.17190/AMF/1246104
SRS	31.817294	-110.850801	1169	19.4	388	WSA	Bsk	2011-2018	10.17190/AMF/1660351
Wdn	40.7838	-106.2618	2469	3.3	336.55	OSH	Bsh	2006-2008	10.17190/AMF/1246832
Whs	31.7438	-110.0522	1370	17.6	320	OSH	Bsk	2007-2020	10.17190/AMF/1246113
Wjs	34.4255	-105.8615	1931	15.2	361	SAV	Bsk	2007-2021	10.17190/AMF/1246120
Wkg	31.7365	-109.9419	1531	15.64	407	GRA	Bsk	2004-2020	10.17190/AMF/1246112

Extended Data Table 2 | Remote sensing products used and details regarding the basic method for flux estimation, the frequency of flux estimates, and the spatial resolution of the gridded products

Product	Method	Frequency	Resolution	Reference
MODIS GPP (MOD17A2GF)	Light-use efficiency	8-day	500 m	Running et al. 2004[51]
SMAP L4C GPP	Light-use efficiency	Daily	9 km	Jones et al. 2017[52]
FluxSat GPP	Machine learning	Daily	0.05°	Joiner & Yoshida 2020[53]
MODIS ET (MOD16A2GF)	Penman-Monteith	8-day	500 m	Mu et al. 2011[54]
GLEAM ET	Priestley-Taylor	Daily	0.25°	Martens et al. 2017[55]

Extended Data Table 3 | R^2 values between daily SMAP surface and root-zone VWC and in situ daily mean VWC across depths at each flux tower site. The final row indicates the mean R^2 across all sites. Empty values indicate either that no in situ soil moisture data were present at that depth for that site, or that the flux tower record did not overlap the SMAP record (2015 – present)

Site	SMAP Surface VWC				SMAP Root-zone VWC			
	Shallow	Shallow-mid	Middle	Deep	Shallow	Shallow-mid	Middle	Deep
ADR	0.004				0.028			
Aud								
CdM	0.097	0.045	0.058	0.042	0.174	0.026	0.046	0.03
CMW	0.54	0.448	0.515	0.025	0.59	0.568	0.585	0.082
Cop								
Jo1	0.307	0.084	0.05		0.411	0.117	0.104	
Jo2	0.211	0.027	0.04		0.279	0.063	0.027	
LS1								
LS2								
Mpj								
Rls	0.619			0.532	0.661			0.575
Seg								
Ses								
SRC								
SRG	0.397	0.323		0.001	0.521	0.556		0.022
SRM	0.501	0.449	0.217	0.041	0.607	0.631	0.439	0.112
SRS	0.45	0.414	0.356	0.172	0.66	0.645	0.621	0.352
Wdn								
Whs	0.406		0.032	0.112	0.63		0.15	0.146
Wjs								
Wkg	0.366	0.3	0.003		0.413	0.37	0.017	
Mean	0.354	0.261	0.159	0.132	0.452	0.372	0.249	0.188